First Example of ZnO−TiO_2 Nanocomposites by Chemical Vapor Deposition: Structure, Morphology, Composition, and Gas Sensing Performances

Davide Barreca,*,† Elisabetta Comini,‡ Angelo P. Ferrucci,§ Alberto Gasparotto,§ Chiara Maccato,§ Cinzia Maragno,§ Giorgio Sberveglieri,‡ and Eugenio Tondello§

ISTM-CNR and INSTM, Department of Chemistry, Padova University, Via Marzolo, 1-35131 Padova, Italy, INFM-CNR, SENSOR, Department of Chemistry and Physics, Brescia University, Via Valotti, 9-25133 Brescia, Italy, and Department of Chemistry, Padova University and INSTM, Via Marzolo, 1-35131 Padova, Italy

Received July 24, 2007. Revised Manuscript Received September 4, 2007

ZnO−TiO_2 nanocomposites were synthesized by an innovative chemical vapor deposition (CVD) strategy, based on the initial growth of ZnO nanoplatelets (host) and the subsequent dispersion of TiO_2 nanoparticles (guest). $Ti(O^iPr)_2(dpm)_2$ and $Zn(hfa)_2$·TMEDA (O^iPr: iso-propoxy; dpm: 2,2,6,6-tetramethyl-3,5-heptanedionate; hfa: 1,1,1,5,5,5-hexafluoro-2,4-pentanedionate; and TMEDA: *N*,*N*,*N*′,*N*′-tetramethylethylenediamine) were adopted as Ti and Zn molecular sources, respectively. The syntheses were performed in nitrogen plus wet oxygen atmospheres at relatively low temperatures (350−400 °C) on Si(100) and Al_2O_3 substrates, avoiding ex-situ thermal treatment to preserve the chemical identity of the host and guest phases. The process resulted in the formation of ZnO−TiO_2 nanocomposite deposits with an average thickness of 140 nm, whose characteristics were directly affected by the host matrix porosity and the guest amount and dispersion, tailored by varying the TiO_2 deposition time. In this framework, particular attention was devoted to the investigation of the composite chemico-physical properties as a function of the adopted processing parameters. Furthermore, the gas sensing performances of the nanocomposites in the detection of volatile organic compounds (CH_3COCH_3, CH_3CH_2OH, and CO) resulted in being directly dependent on their composition and morphology, revealing better performances than the pristine ZnO systems. These results disclose intriguing perspectives for the development of sensing devices for environmental purposes and food control monitoring.

Introduction

The design and preparation of nanocomposites based on semiconducting oxides is an important goal for the obtainment of improved functional performances in several advanced fields.[1−6] Among mixed semiconductor systems, binary ZnO−TiO_2 nanocomposites have received considerable interest, thanks to the possibility of achieving a synergistic combination of the peculiar component characteristics,[7,8] such as the high reactivity of TiO_2 and the large exciton binding energy of ZnO (60 meV).[9,10] In particular, electron and hole transfer processes between their conduction and valence bands result in a better separation of photogenerated carriers with respect to the single oxides, disclosing interesting perspectives for photocatalytic applications.[3,4,7,8,11,12] In addition, improved functional performances in sensing devices for volatile organic compounds (VOCs) have been reported.[13] In fact, despite the fact that ZnO systems have been widely employed in solid-state gas sensors,[5,14−16] two main drawbacks in their use arise from the relatively low selectivity and high operating temperatures.[17−20] Such disadvantages can be overcome by the introduction of TiO_2 in

* Corresponding author tel: +39 049 8275170; fax: +39 049 8275161; e-mail: davide.barreca@unipd.it.
† ISTM-CNR.
‡ Brescia University.
§ Padova University.

(1) Wang, Z.-S.; Huang, C.-H.; Huang, Y.-Y.; Hou, Y.-J.; Xie, P.-H.; Zhang, B.-W.; Chen, H.-M. *Chem. Mater.* **2001**, *13*, 678.
(2) Abrams, B. L.; Wilcoxon, J. P. *Crit. Rev. Solid State Mater. Sci.* **2005**, *30*, 153.
(3) Marcì, G.; Augugliaro, V.; López-Muñoz, M. J.; Martín, C.; Palmisano, L.; Rives, V.; Schiavello, M.; Tilley, R. J. D.; Venezia, A. M. *J. Phys. Chem. B* **2001**, *105*, 1026.
(4) Kandavelu, V.; Kastien, H.; Thampi, K. R. *Appl. Catal., B* **2004**, *48*, 101.
(5) Kwon, T.-H.; Park, S.-H.; Ryu, J.-Y.; Choi, H.-H. *Sens. Actuators, B* **1998**, *46*, 75.
(6) Keis, K.; Roos, A. *Opt. Mater.* **2002**, *20*, 35.
(7) Yang, S. G.; Quan, X.; Li, X. Y.; Liu, Y. Z.; Chen, S.; Chen, G. H. *Phys. Chem. Chem. Phys.* **2004**, *6*, 659.
(8) Wu, W.; Cai, Y.-W.; Chen, J.-F.; Shen, S.-L.; Martin, A.; Wen, L.-W. *J. Mater. Sci.* **2006**, *41*, 5845.
(9) Wang, X.; Summers, C. J.; Wang, Z. L. *Nano Lett.* **2004**, *4*, 423.
(10) Kim, S. W.; Fujita, S.; Park, H. K.; Yang, B.; Kim, H. K.; Yoon, D. H. *J. Cryst. Growth* **2006**, *292*, 306.
(11) Marcì, G.; Augugliaro, V.; López-Muñoz, M. J.; Martín, C.; Palmisano, L.; Rives, V.; Schiavello, M.; Tilley, R. J. D.; Venezia, A. M. *J. Phys. Chem. B* **2001**, *105*, 1033.
(12) Wang, X.-T.; Zhong, S.-H.; Xiao, X.-F. *J. Mol. Catal. A: Chem.* **2005**, *229*, 87.
(13) Zhu, B. L.; Xie, C. S.; Wang, W. Y.; Huang, K. J.; Hu, J. H. *Mater. Lett.* **2004**, *58*, 624.
(14) Kwon, T. H.; Ryu, J. Y.; Choi, W. C.; Kim, S. W.; Park, S. H.; Choi, H. H.; Lee, M. K. *Sens. Mater.* **1999**, *11*, 257.
(15) Eranna, G.; Joshi, B. C.; Runthala, D. P.; Gupta, R. P. *Crit. Rev. Solid State Mater. Sci.* **2004**, *29*, 111.
(16) Comini, E. *Anal. Chim. Acta* **2006**, *568*, 28.
(17) Baratto, C.; Sberveglieri, G.; Onischuk, A.; Caruso, B.; di Stasio, S. *Sens. Actuators, B* **2004**, *100*, 261.
(18) Xu, H.; Liu, X.; Cui, D.; Li, M.; Jiang, M. *Sens. Actuators, B* **2006**, *114*, 301.
(19) de Lacy Costello, B. P. J.; Ewen, R. J.; Ratcliffe, N. M.; Sivanand, P. S. *Sens. Actuators, B* **2003**, *92*, 159.

10.1021/cm701990f CCC: $37.00
Published on Web 10/12/2007

ZnO matrices, resulting in improved sensor sensitivity and selectivity, since titanium dioxide behaves as a catalytic promoter of the involved chemical processes.[5,13,14]

The functional properties of ZnO−TiO$_2$ nanocomposites for applications in the previously mentioned fields can be suitably tuned by tailoring their morphological and structural features, that, in turn, have an appreciable influence on the interactions with the target species present in the surroundings.[20−22] To control the resulting ZnO−TiO$_2$ properties, an adequate choice of the synthesis and processing parameters plays a key role. Previous literature reports have focused on the preparation of ZnO−TiO$_2$ systems by various techniques, including sol−gel,[7,8,22,23] magnetron sputtering,[5,14,24,25] evaporation and thermal oxidation,[26,27] thermal treatment of powders,[13,28] and liquid phase routes.[3,12,29−32] In most cases, the occurrence of solid-state reactions, leading to the formation of ternary Zn−Ti−O species,[8,13,23,28,29] has been observed. Nevertheless, to favorably exploit the combination between ZnO and TiO$_2$ properties, such phenomena have to be avoided through a proper choice of mild bottom-up synthetic routes.

Among the various techniques, chemical vapor deposition (CVD) offers significant advantages, due to its inherent versatility and the possibility of operating under relatively soft conditions. Nonetheless, to the best of our knowledge, only one work on the CVD of zinc titanate films is available in the literature to date,[33] while the synthesis of ZnO−TiO$_2$ nanocomposites by this technique has never been reported. In the past few years, our research group has been focused on the use of porous substrates as hosts for the CVD of suitable guest phases for the obtainment of oxide nanosystems with tailored properties.[34−37] More recently, we have demonstrated that CVD processes under suitable conditions can lead to the formation of ZnO nanoplatelets (NPTs) endowed with a high surface/volume ratio, an interesting feature for their subsequent photocatalytic and gas sensing applications.[38] On the basis of these results, in the present work, ZnO−TiO$_2$ nanocomposites have been synthesized for the first time by thermal CVD, adopting Ti(O^{i}Pr)$_2$(dpm)$_2$ and Zn(hfa)$_2$·TMEDA as Ti and Zn molecular sources, respectively. In particular, while the use of the Ti precursor in CVD processes is well-established,[39−42] the Zn compound, synthesized for the first time by Marks et al.,[43] has been employed only recently by some of us.[38] Main attention has been devoted to the obtainment of porous ZnO NPTs to be used as host matrices for the subsequent dispersion of TiO$_2$ nanoparticles, resulting in a suitable morphology for the development of sensing devices. After a morphological, structural, and compositional characterization of the obtained systems as a function of the synthesis conditions, their gas sensing properties have been tested in the detection of VOCs, in particular, CH_3COCH_3, CH_3CH_2OH, and CO, which are of interest for environmental purposes and food control monitoring.[17,44,45] It is worth noticing that only a few studies on the sensing properties of ZnO−TiO$_2$-based systems have been performed to date.[5,14,46,47]

Experimental Procedures

Synthesis. Ti(O^{i}Pr)$_2$(dpm)$_2$ (99.99%) was purchased from Aldrich and used without further purification. Conversely, Zn(hfa)$_2$·TMEDA was synthesized following a literature procedure.[43] CVD experiments were performed in a homemade cold-wall system[48] by sequential deposition of single phase ZnO and TiO$_2$ under nitrogen plus wet oxygen atmospheres, adopting optimized pressure and flow rate conditions [total pressure = 10 mbar; for ZnO: $\Phi(N_2) = 40$ sccm $= \Phi(O_2 + H_2O)$ and deposition time = 60 min; for TiO$_2$: $\Phi(N_2) = 40$ sccm and $\Phi(O_2 + H_2O) = 80$ sccm]. The vaporization temperatures for the Zn and Ti precursors were set at 60 and 90 °C, respectively. In particular, the O_2 flow was introduced in the reaction chamber after passing through a water reservoir maintained at 50 °C (H_2O partial pressure ≈ 1.5 mbar).[48] The gas lines connecting the water and precursor reservoirs to the reaction chamber were heated to 110 °C to avoid undesired condensation phenomena. Beside *p*-type Si(100) wafers, polycrystalline Al_2O_3 slides were also used as substrates in view of gas sensing tests, and both were suitably cleaned prior to deposition to minimize the

(20) Ryu, H.-W; Park, B. S.; Akbar, S. A.; Lee, W.-S.; Hong, K.-J.; Seo, Y.-J.; Shin, D.-C.; Park, J.-S.; Choi, G.-P. *Sens. Actuators, B* **2003**, *96*, 717.
(21) Epifani, M.; Diaz, R.; Arbiol, J.; Comini, E.; Sergent, N.; Pagnier, T.; Siciliano, P.; Faglia, G.; Morante, J. R. *Adv. Funct. Mater.* **2006**, *16*, 1488.
(22) Tai, W.-P.; Kim, J.-G.; Oh, J.-H. *Sens. Actuators, B* **2003**, *96*, 477.
(23) Ocaña, M.; Hsu, W. P.; Matijevic, E. *Langmuir* **1991**, *7*, 2911.
(24) Lin, S.-S; Huang, J.-L.; Lii, D.-F. *Surf. Coat. Technol.* **2005**, *190*, 372.
(25) Lu, Y.-M.; Chang, C.-M.; Tsai, S.-I.; Wey, T.-S. *Thin Solid Films* **2004**, *447−448*, 56.
(26) Dakhel, A. A. *Appl. Phys. A* **2003**, *77*, 677.
(27) Saeki, I.; Setaka, J.; Furuichi, R.; Konno, H. *J. Electroanal. Chem.* **1999**, *464*, 238.
(28) Wang, C.; Xu, B.-Q.; Wang, X.; Zhao, J. *J. Solid State Chem.* **2005**, *178*, 3500.
(29) Chang, Y.-S.; Chang, Y.-H.; Chen, I.-C.; Chen, G.-J.; Chai, Y.-L. *J. Cryst. Growth* **2002**, *243*, 319.
(30) Yang, H. G.; Zeng, H. C. *J. Am. Chem. Soc.* **2005**, *127*, 270.
(31) Mane, R. S.; Lee, W. J.; Pathan, H. M.; Han, S. H. *J. Phys. Chem. B* **2005**, *109*, 24254.
(32) Kim, S.-S.; Yum, J.-H.; Sung, Y.-E. *J. Photochem. Photobiol., A* **2005**, *171*, 69.
(33) Chen, Z.-X; van der Eyden, J.; Koot, W.; van den Berg, R.; van Mechelen, J.; Derking, A. *J. Am. Ceram. Soc.* **1995**, *78*, 2993.
(34) Armelao, L.; Barreca, D.; Bottaro, G.; Gasparotto, A.; Tondello, E.; Ferroni, M.; Polizzi, S. *Chem. Vap. Deposition* **2004**, *10*, 257.
(35) Armelao, L.; Barreca, D.; Bottaro, G.; Gasparotto, A.; Maragno, C.; Tondello, E. *Chem. Mater.* **2005**, *17*, 427.
(36) Armelao, L.; Barreca, D.; Bottaro, G.; Gasparotto, A.; Maragno, C.; Tondello, E.; Sada, C. *J. Nanosci. Nanotechnol.* **2005**, *5*, 781.
(37) Armelao, L.; Barreca, D.; Bottaro, G.; Gasparotto, A.; Maragno, C. *Chem. Vap. Deposition* **2007**, *13*, 112.
(38) Barreca, D.; Ferrucci, A. P.; Gasparotto, A.; Maccato, C.; Maragno, C.; Tondello, E. *Chem. Vap. Deposition* **2007**, in press.
(39) Ryu, H.-K; Heo, J. S.; Cho, S.-I.; Moon, S. H. *J. Electrochem. Soc.* **1999**, *146*, 1117.
(40) Turgambaeva, A. E.; Krisyuk, V. V.; Sysoev, S. V.; Igumenov, I. K. *Chem. Vap. Deposition* **2001**, *7*, 121.
(41) Lo Nigro, R.; Toro, R. G.; Malandrino, G.; Fragalà, I. L.; Losurdo, M.; Giangregorio, M. M.; Bruno, G.; Raineri, V.; Fiorenza, P. *J. Phys. Chem. B* **2006**, *110*, 17460.
(42) Baunemann, A.; Hellwig, M.; Varade, A.; Bhakta, R. K.; Winter, M.; Shivashankar, S. A.; Fischer, R. A.; Devi, A. *Dalton Trans.* **2006**, 3485.
(43) Ni, J.; Yan, H.; Wang, A.; Yang, Y.; Stern, C. L.; Metz, A. W.; Jin, S.; Wang, L.; Marks, T. J.; Ireland, J. R.; Kannewurf, C. R. *J. Am. Chem. Soc.* **2005**, *127*, 5613.
(44) Gong, H.; Hu, J. Q.; Wang, J. H.; Ong, C. H.; Zhu, F. R. *Sens. Actuators, B* **2006**, *115*, 247.
(45) Barreca, D.; Gasparotto, A.; Maccato, C.; Maragno, C.; Tondello, E.; Comini, E.; Sberveglieri, G. *Nanotechnology* **2007**, *18*, 125502.
(46) Park, S. H.; Choi, H. H.; Kwon, T. H. *Sens. Mater.* **1996**, *8*, 485.
(47) Mineiro, S. L.; Nono, M. C. A.; Kuranaga, C.; Silva, M. D. *Mater. Sci. Forum* **2005**, *498−499*, 293.
(48) Barreca, D.; Gasparotto, A.; Maragno, C.; Tondello, E.; Bontempi, E.; Depero, L. E.; Sada, C. *Chem. Vap. Deposition* **2005**, *11*, 426.

Table 1. Synthesis Conditions Adopted for the Preparation of ZnO−TiO_2 Nanocomposites on Si(100) and Al_2O_3 Substrates

sample	ZnO deposition (I)	TiO_2 deposition (II)
1	$T = 350$ °C	10 min
2	$T = 400$ °C	10 min
3	$T = 350$ °C	30 min
4	$T = 400$ °C	30 min

presence of surface contaminants. On the basis of previous results,[38] for ZnO NPTs, the deposition temperature was varied between 350 and 400 °C (see Table 1, I) since these values corresponded to the highest system porosity, a favorable characteristic for the subsequent TiO_2 dispersion. With regard to titanium oxide, its amount was varied by changing its deposition time between 10 and 30 min (see Table 1, II). Higher values were discarded to avoid a complete occlusion of the zinc oxide matrix and to obtain a tailored dispersion of titanium dioxide particles. Conversely, its growth temperature was kept constant at 400 °C for all TiO_2 depositions since preliminary experiments on the bare substrates indicated it as the minimum adoptable value for the obtainment of crystalline anatase. The use of higher temperatures was not taken into account to minimize undesired modifications of the underlying ZnO host matrices. The reproducibility of the obtained results was ascertained by means of repeated deposition runs adopting the same experimental parameters.

In all cases, no ex-situ thermal treatments were performed to prevent solid-state reactions, leading ultimately to the formation of zinc titanate ternary phases.[23,27,29] Even the use of a soft annealing to promote TiO_2 dispersion in the ZnO matrices was discarded, to avoid detrimental nanocomposite alterations, such as their compaction. For comparison of the gas sensing performances, bare ZnO NPTs were also prepared on Al_2O_3 substrates.

Characterization. Glancing incidence X-ray diffraction (GIXRD) patterns were recorded by a Bruker D8 Avance diffractometer equipped with a Göbel mirror and a Cu Kα source (40 kV, 40 mA), at a fixed incidence angle of 0.5°. The average crystallite dimensions were estimated by means of the Scherrer equation.

Field emission-scanning electron microscopy (FE-SEM) measurements were performed using a Zeiss SUPRA 40VP instrument, equipped with an Oxford INCA x-sight X-ray detector for energy dispersive X-ray spectroscopy (EDXS) measurements. Plane-view and cross-sectional images were acquired adopting an acceleration voltage between 10 and 20 kV.

A PerkinElmer Φ 5600ci apparatus with non-monochromatized Mg Kα radiation (1253.6 eV) was used for the XPS (X-ray photoelectron spectroscopy) and XE-AES (X-ray excited-auger electron spectroscopy) measurements, at working pressures lower than 10^{-9} mbar. The reported binding energies (BEs; standard deviation = ±0.2 eV) were corrected for charging assigning to the adventitious C1s line a BE of 284.8 eV.[49] After a Shirley-type background subtraction, the raw spectra were fitted using a nonlinear least-squares fitting program adopting Gaussian−Lorentzian shapes for all peaks. The atomic compositions were evaluated using sensitivity factors as provided by Φ V5.4A software. Depth profiling was carried out by Ar^+ sputtering at 2.5 kV, with an argon partial pressure of 5×10^{-8} mbar. The root-mean-square scatter on each concentration value was assumed to be 15%, according to previous literature reports.[49,50]

For the fabrication of sensors, a platinum interdigitated electrode structure[45] and a Pt heater were sputtered over the ZnO/TiO_2 nanocomposite systems and on the backside of the alumina substrate, respectively. The sensor operating temperature was achieved by applying a constant voltage to the heater, using the same Pt resistance also as a thermometer. The flow-through technique[45] was used to test the gas sensing properties. A constant synthetic air flow (0.3 L/min) at atmospheric pressure was used as a carrier gas for the dispersion of the analyte gases in the desired concentration. All measurements were performed in a temperature-stabilized sealed chamber at 20 °C under a constant humidity level of 40%, adopting the volt-amperometric technique at a constant bias voltage (1 V). The sensing properties were characterized at working temperatures between 200 and 400 °C. Before measurements, all samples were pre-stabilized at the working temperature for 8 h. In the case of reducing gases and *n*-type semiconductors, as in the present case, the sensor response was defined as the relative conductance variation upon gas exposure.[45] The estimated uncertainty on the response values was ±5%. The response time was described as the interval required for sample conductance to reach 90% of the equilibrium value following an injection of the test gas, while the recovery time was the one necessary for the sample to return to 10% above the original conductance in air after releasing the analyte.[13]

Results and Discussion

In this work, particular attention was devoted to the obtainment of ZnO−TiO_2 nanocomposites under sufficiently mild conditions to prevent the formation of zinc titanates. To ascertain the absence of ternary Zn−Ti−O phases, all the obtained specimens were preliminarily subjected to GIXRD analysis (Figure 1). Irrespective of the adopted deposition conditions, all the recorded patterns were dominated by the Bragg reflections of ZnO in the wurtzite hexagonal phase,[51] located at $2\vartheta = 34.5°$ (002), 36.4° (101), and 47.7° (102). As already reported,[38] the higher intensity of the (002) peak with respect to the other ones suggested an orientation with the *c*-axis (i.e., the ⟨001⟩ direction) almost normal to the substrate surface. Such a phenomenon, frequently observed in the case of ZnO systems, was mainly explained by the anisotropic ⟨001⟩ growth arising from the peculiar zinc oxide structure.

Despite a slight decrease of the total diffracted intensity with respect to the bare ZnO systems, no significant modifications of ZnO peak positions and relative intensities were observed upon titanium dioxide growth. Concerning Si(100)-supported samples (Figure 1a), for a TiO_2 deposition time of 30 min (samples 3 and 4), a weak diffraction peak located at $2\vartheta = 25.3°$ was observed and attributed to (101) anatase TiO_2 planes.[52] It is worthwhile observing that the (101) anatase peak displayed a higher intensity when the underlying zinc oxide matrix was deposited at 400 °C (sample 4). This feature was ascribed to a lowered ZnO porosity with respect to the 350 °C grown sample, inducing a more pronounced titania structural ordering in the outermost sample layers.[38] The lack of clearly detectable TiO_2 reflections for samples 1 and 2, obtained with 10 min deposition, was ascribed both to a lowered material amount and to an increased titania dispersion, resulting in an intrinsic structural disorder. These predictions were indeed confirmed by compositional analyses.

(49) Briggs, D.; Seah, M. P. *Practical Surface Analysis*, 2nd ed.; John Wiley and Sons: New York, 1990.
(50) Tougaard, S. *Surf. Interface Anal.* **1998**, *26*, 249.
(51) Pattern No. 36-1451, JCPDS, 2000.
(52) Pattern No. 21-1272, JCPDS, 2000.

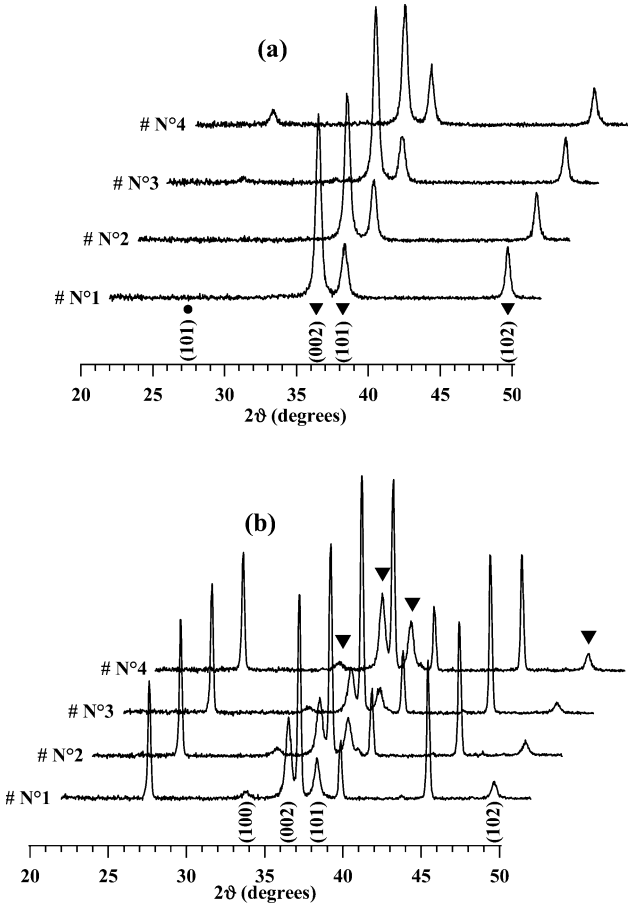

Figure 1. GIXRD patterns of ZnO−TiO_2 nanocomposites synthesized according to Table 1, deposited on (a) Si(100) and (b) Al_2O_3. In the latter case, the most intense diffraction peaks are due to the substrate. ZnO wurtzite (▼) and TiO_2 anatase (●) peaks have been labeled.

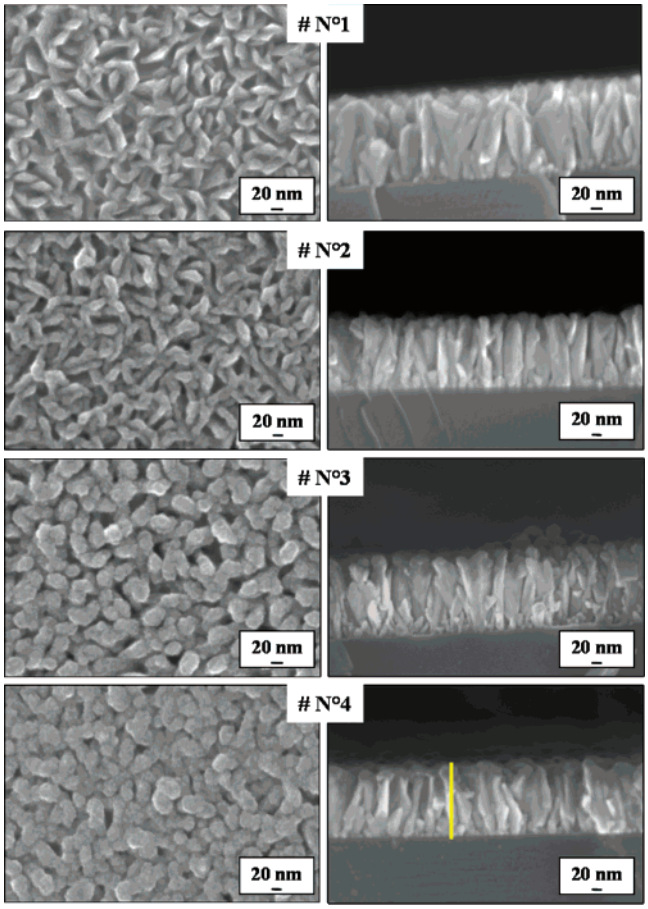

Figure 2. Plane-view (left) and cross-sectional (right) FE-SEM micrographs of ZnO−TiO_2 nanocomposites deposited on Si(100) adopting the conditions in Table 1. The line marked for sample 4 corresponds to the EDXS scans reported in Figure 3.

As regards the systems deposited on Al_2O_3 (Figure 1b), two main differences in GIXRD patterns with respect to Si(100)-supported samples could be highlighted. The first concerned the appearance of a weak peak located at $2\vartheta = 33.8°$ due to (100) ZnO planes, suggesting that the use of rougher substrates (average roughness = 70 and 0.4 nm for Al_2O_3 and Si(100) substrates, respectively)[53] resulted in a slightly less selective anisotropic growth of zinc oxide systems. Furthermore, irrespective of the synthesis conditions, no titania signals were ever detected. On the basis of FE-SEM observations, this result was ascribed to a higher TiO_2 structural disorder, attributed, in turn, to the corrugation of the Al_2O_3 substrate and, consequently, of the supported ZnO matrices.

Such observations, along with XPS and XE-AES data, confirmed that the adopted processing conditions were sufficiently mild to ensure the formation of ZnO−TiO_2 nanocomposites, excluding the occurrence of chemical reactions between them. This result agreed to a good extent with previous literature works, reporting the onset of zinc titanate formation for temperatures of 600 °C.[27,29] Irrespective of the synthesis conditions, the average crystallite sizes for zinc oxide were close to 20 nm. As regards TiO_2, a similar value was obtained for sample 4 on Si(100), the only one displaying a sufficient peak intensity to perform this calculation.

Subsequently, attention was devoted to investigating the interplay between the processing parameters and the resulting system morphology as a function of the adopted substrates. To this aim, FE-SEM analyses provided valuable information, as displayed in Figures 2 and 3. As concerns Si(100)-supported nanocomposites (Figure 2), the main factor influencing the system morphology was the TiO_2 process duration and, hence, the overall titania content. In fact, for a deposition time of 10 min (samples 1 and 2), plane-view images displayed high density intertwined NPTs 60 nm long, with an average thickness of 10 nm, whose shape and distribution closely resembled those obtained for the pristine ZnO-based systems.[38] The increased NPTs thickness, from ≈5 to 20 nm, upon titania deposition, was related to a conformal coverage of ZnO NPTs by interconnected TiO_2 particles. Such a peculiar TiO_2 morphology was related to a synergistic combination of a three-dimensional growth mode, likely induced by the presence of surface −OH groups acting as nucleation sites,[34,37] and the typical conformal coverage characterizing CVD techniques. In a different way, an increase of the TiO_2 deposition time to 30 min (samples 3 and 4) resulted in a morphology evolution from NPTs to rounded and denser multi-granular particles (mean size = 50 nm), whose formation was clearly related to the higher

(53) Barreca, D.; Buchberger, A.; Daolio, S.; Depero, L. E.; Fabrizio, M.; Morandini, F.; Rizzi, G. A., Sangaletti, L.; Tondello, E. *Langmuir* **1999**, *15*, 4537.

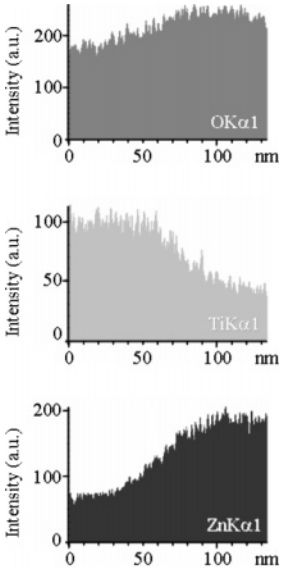

Figure 3. Representative EDXS scans along the line marked in Figure 3 for OKα1, TiKα1, and ZnKα1 X-ray signals. The abscissa value increases from the sample surface to the deposit−substrate interface.

TiO_2 deposited amount. In fact, it is worth noting that the GIXRD patterns of these samples (see previous discussion and Figure 1a) exhibited the main anatase peak.

Further differences in the morphological features of the obtained systems arose from the deposition temperature of the ZnO matrix (350 or 400 °C). In fact, the present nanocomposites were characterized by a higher compaction upon titania deposition on ZnO obtained at 400 °C (Figure 2; compare samples 2 and 4 with 1 and 3, respectively). As already mentioned, such a feature was related to the lowered porosity of zinc oxide matrices grown at higher temperatures and anticipated a different degree of titania dispersion as a function of the adopted synthesis conditions. Furthermore, all the plane-view micrographs reported in Figure 2 confirmed that the adopted processing parameters enabled us to prevent a complete suppression of the pristine system porosity.[38]

Similar to the case of pure ZnO,[38] the cross-sectional images in Figure 2 revealed the presence of pseudo-columnar structures aligned almost vertically with respect to the substrate surface, indicating a direct correlation with the preferential ⟨001⟩ orientation observed by GIXRD analysis. At variance with plane-view images, the nanocomposite cross-sectional structures were not strongly influenced by the adopted synthesis parameters, indicating that titania deposition did not induce a drastic alteration of the parent ZnO matrices. Correspondingly, an average sample thickness of 140 nm was measured for all specimens.

Preliminary important information on the local chemical composition was obtained by EDXS, performing different line-scans along the system thickness and obtaining complementary results with respect to those yielded by XPS depth profiling.[45] Representative O, Ti, and Zn trends are proposed in Figure 3. A relevant feature characterizing all the obtained specimens was Ti penetration throughout the nanodeposit thickness, owing to a vapor infiltration of the Ti precursor and related fragments in the underlying ZnO matrix. Notably, for a TiO_2 deposition time of 30 min (samples 3 and 4), a Ti accumulation in an external region ≈60 nm thick could be observed, followed by its subsequent decrease on going toward the substrate surface. Conversely, for a TiO_2 deposition time of 10 min (samples 1 and 2, data not shown), a lower Ti content and a more uniform titanium distribution throughout the nanodeposit thickness were obtained.

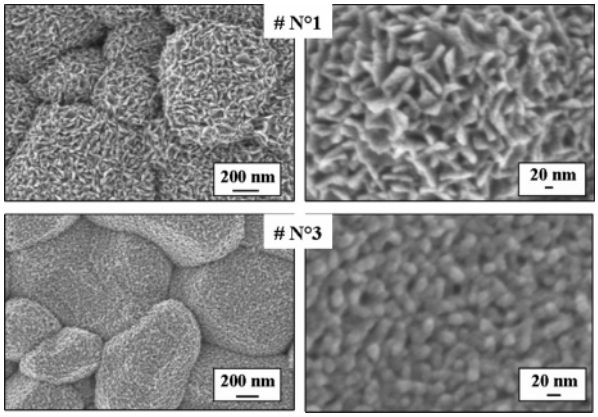

Figure 4. Representative plane-view FE-SEM micrographs of $ZnO-TiO_2$ nanocomposites deposited on Al_2O_3 adopting the conditions in Table 1.

Irrespective of the specific line-scan position, similar results were obtained for the same sample, pointing out a remarkable lateral homogeneity of the system composition. These findings agree to a good extent with in-depth XPS analysis.

On the basis of the obtained results, deposition of $ZnO-TiO_2$ specimens was subsequently performed on polycrystalline Al_2O_3 for gas sensing measurements. The corresponding plane-view FE-SEM images (Figure 4) revealed an appreciable dependence of the system morphology on the nature of the adopted substrate. In fact, all the micrographs were dominated by the presence of Al_2O_3 particles with sizes ranging between 500 and 700 nm, uniformly covered by $ZnO-TiO_2$ nanocomposites. This peculiar morphology is likely to be associated with a higher effective surface area than that of the homologous Si(100)-supported systems, an interesting feature in view of the eventual gas sensing applications.

Beyond the major differences related to the substrate corrugation, a detailed comparison of Figures 2 and 4 indicates the occurrence of similar nanostructures for samples synthesized using the same experimental conditions, suggesting the occurrence of analogous nucleation and growth mechanisms. In particular, for a TiO_2 deposition time of 10 min (sample 1), entangled NPTs with shape and dimensions very similar to those obtained on Si(100) were obtained (compare Figure 2). An increase of the titania deposition time to 30 min (sample 3) resulted in the formation of densely packed globular aggregates, whose features were almost independent of the deposition conditions of the underlying ZnO matrix.

Further information on the surface and in-depth chemical composition was obtained by XPS. In all cases, surface analysis revealed the presence of Ti, O, and C signals, while Zn photopeaks could be unambiguously detected only for a titania deposition time of 10 min. Such a phenomenon proved that, for a TiO_2 growth duration of 30 min, a uniform

conformal coverage of ZnO nanostructures by TiO_2 particles took place.

The presence of carbon could be related to adventitious contamination arising from air exposure, since the pertaining signals were reduced to noise level after a mild Ar^+ sputtering. Such a phenomenon indicated a clean decomposition pattern of both the adopted Zn and Ti CVD precursors, in agreement with previous results.[38] As regards the Ti2p$_{3/2}$ photoelectron signal, its BE was centered at 458.7 eV [full width at half-maximum (fwhm) = 1.7 eV], a value very close to that previously reported in the literature for titania.[3,32,54] The O1s surface signal was deconvoluted by means of two bands located at BE = 530.2 (fwhm = 1.7 eV) and 531.5 eV (fwhm = 2.3 eV), ascribed, respectively, to lattice oxygen and -OH species,[3,32,38] the latter being related to both atmospheric exposure and the presence of water vapor in the reaction atmosphere.

For a TiO_2 deposition time of 10 min (samples 1 and 2), the presence of Zn peaks could be observed. In particular, the Zn2p$_{3/2}$ signal (BE = 1022.0 eV) agreed with the presence of zinc(II) oxide,[3,32] which was further confirmed by evaluating the Zn auger α parameter (α = 2010.3 eV).[38,54] These results, in conjunction with the GIXRD ones, confirmed that both ZnO and TiO_2 maintained their chemical identity under the adopted conditions. For samples 1 and 2, the Ti/Zn surface atomic ratios yielded values close to 1.5 and 5.0, respectively. In agreement with the previous considerations (see comments to Figure 2), this difference could be related to the greater porosity of the underlying ZnO deposited at 350 °C, which is likely to result in an improved TiO_2 dispersion in the inner sample layers, resulting, in turn, in a lower Ti/Zn surface ratio (sample 1). This prediction was indeed confirmed by XPS depth profiling, which yielded important information on the mutual ZnO/TiO_2 distribution in the obtained nanocomposites as a function of the synthesis parameters. As a matter of fact, the atomic percentages versus erosion time trends did not show an appreciable dependence on the adopted growth surface but were significantly affected by the synthesis conditions. Figure 5 displays the profiles obtained for samples deposited on Si(100). The existence of a relatively broad interface with the Si substrate, characterized by the co-presence of Zn, Ti, and Si species, could be traced back to the peculiar system morphology, resulting in apparent intermixing effects upon Ar^+ erosion.

Irrespective of the adopted experimental conditions, titania penetration throughout ZnO matrices was evidenced and attributed to the synergy between the system porosity and the peculiar infiltration power of CVD techniques, as already evidenced in the discussion of EDXS line-scan results (compare Figure 3). In this context, a further synergistic contribution could arise from the presence of −OH groups in the ZnO matrix pores, acting as catalytic sites for the Ti precursor decomposition[34,37] and further favoring TiO_2 dispersion in the inner system layers by a sort of "dragging" effect. A careful inspection of the profiles suggested a

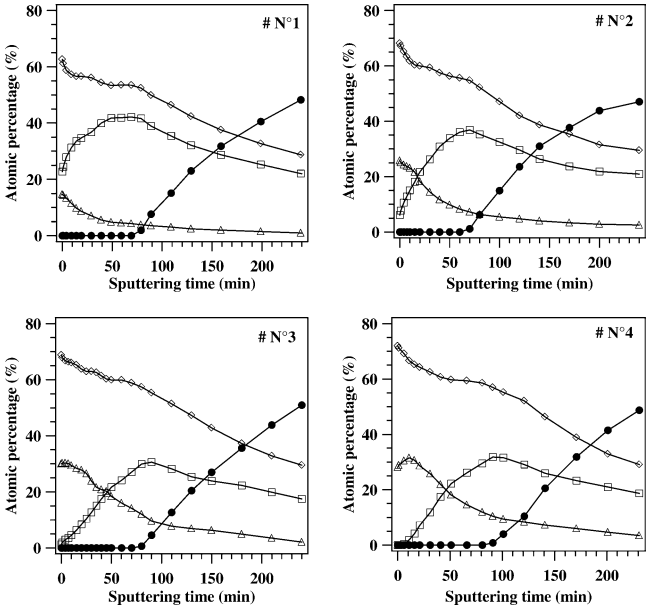

Figure 5. XPS depth profiles for ZnO−TiO_2 nanocomposites deposited on Si(100) adopting the conditions in Table 1 (● Si, ◇ O, □ Zn, and △ Ti).

dependence of the in-depth elemental distribution on both the TiO_2 deposition time and the growth temperature of the underlying ZnO matrix.

For a titania deposition time of 10 min (samples 1 and 2), a co-presence of Zn and Ti in the outermost layers could be observed, as already anticipated in the discussion of surface data. In particular, for the sample obtained from a ZnO matrix grown at 350 °C (sample 1), zinc oxide resulted in being the prevailing species throughout the investigated depth. The Ti surface percentage was estimated to be 15% at the surface and progressively decreased to 4% after 80 min of erosion, indicating a significant dispersion of TiO_2 throughout the host matrix. On increasing the ZnO growth temperature to 400 °C (sample 2), while keeping constant the TiO_2 deposition time, an external region characterized by TiO_2 accumulation could be evidenced. In fact, the Ti surface content was 25% and decreased to 6% after 80 min of erosion, intersecting the Zn profile at 20 min sputtering. This difference was ascribed to the lower porosity of the underlying host zinc oxide matrix, in accordance with the morphological results.

A considerable modification of the observed profiles took place upon increasing the titania deposition time to 30 min (samples 3 and 4 in Table 1). In this case, the elemental distribution was mainly influenced by the TiO_2 content, rather than by the morphology of the underling ZnO system. For both specimens 3 and 4 (Figure 5), an outer region extending down to ≈50 min erosion and characterized by a titania predominance was observed (surface percentage = 30%), while ZnO resulted in the most abundant phase in the inner sample layers. This result agreed with the observation of anatase peaks in the corresponding GIXRD patterns (see Figure 1a) and the absence of Zn signals in the surface spectra of both samples. In fact, FE-SEM characterization revealed that under these conditions, a uniform conformal coverage of ZnO NPTs by TiO_2 particles took place (compare Figure 2). At variance with structural results, the deposition

(54) Moulder, J. F.; Stickle, W. F.; Sobol, P. W.; Bomben, K. D. *Handbook of X-ray Photoelectron Spectroscopy*; PerkinElmer: Eden Prairie, MN, 1992.

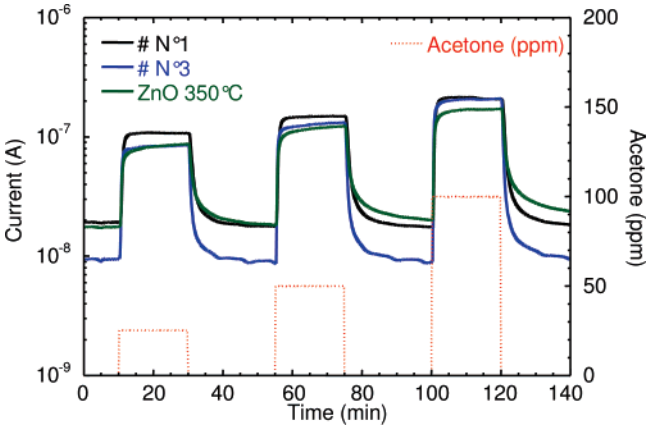

Figure 6. Dynamic response of selected ZnO−TiO_2 nanocomposites (see Table 1) upon exposure to concentration square pulses of acetone at a working temperature of 400 °C. The curve pertaining to a pure ZnO nanosystem is displayed for comparison.

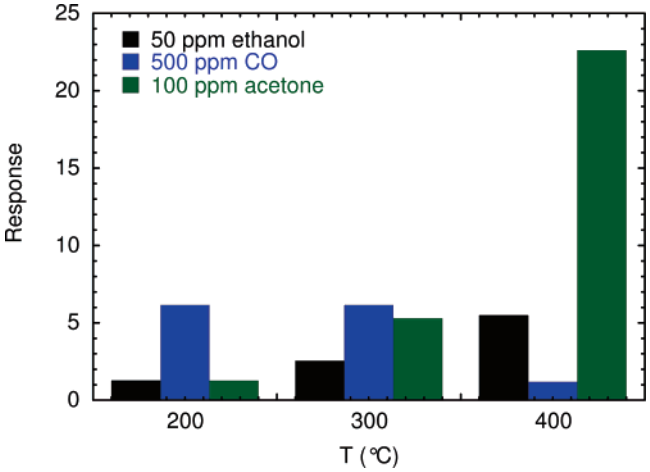

Figure 7. Response of a ZnO−TiO_2 system (sample 3, see Table 1) to selected concentrations of CH_3CH_2OH, CO, and CH_3COCH_3 at different operating temperatures.

temperature of the underlying ZnO matrix did not appreciably affect the in-depth chemical composition of the composite system for a titania deposition time of 30 min (samples 3 and 4).

On the basis of the obtained results, ZnO−TiO_2 nanosystems were subjected to gas sensing tests toward VOCs. In particular, main attention was focused on samples 1 and 3, obtained with a ZnO deposition temperature of 350 °C, which presented an apparent higher porosity and, hence, were more promising in view of gas sensing applications.

Figure 6 compares the dynamic response of ZnO−TiO_2 specimens toward square concentration pulses of CH_3COCH_3 with the response of pure ZnO NPTs obtained at a deposition temperature of 350 °C. Upon gas exposure, the current flowing through the samples increased, in agreement with the behavior expected for *n*-type semiconducting systems and reducing gases.[16,21,45,55] In all cases, the current variation in the presence of the target species was proportional to the analyte concentration, without displaying any saturation effect. The recovery of the air conductance value after sensing tests was almost complete, especially in the case of ZnO−TiO_2 nanocomposites, suggesting the occurrence of reversible interactions between the analytes and the sensor elements. Furthermore, composite systems displayed both response and recovery times on the order of 1 min, lower than those pertaining to pure ZnO NPTs.

It is worth highlighting that the observed current variations were systematically higher for ZnO−TiO_2 nanocomposites with respect to the pristine ZnO matrices, irrespective of the sensing test conditions. In addition, a comparison of the curves pertaining to samples 1 and 3 evidenced a higher current change upon gas exposure in the latter case, suggesting improved gas sensing performances. Such a result, which could be ascribed to the increased TiO_2 amount for specimen 3, agreed to a good extent with previous literature works on the gas sensing properties of thick ZnO−TiO_2 films toward acetone and alcohols, reporting a sensor response proportional to the titania content.[13] Indeed, for all the analyte gases examined in the present work, a higher current variation was observed for samples with the higher TiO_2 amount, indicating a significant beneficial effect of titania addiction on the sensor functional performances. These results could be explained taking into account the detection mechanism of VOCs for ZnO systems, involving chemisorption of atmospheric oxygen on the sensor surface and subsequent reactions of the resulting species with analyte gases, producing electron release.[5,13,16,18,44] Accordingly, the system response was directly influenced by the amount of adsorbed oxygen species and the stabilization of electron−hole pairs, which, in turn, is related to the chemical and physical properties of the sensing system. In particular, TiO_2-containing ZnO composites, thanks to the higher oxygen defect content induced by titania dispersion, are capable of adsorbing oxygen more efficiently than pure ZnO systems,[13] providing superior functional performances. In addition, ZnO−TiO_2 coupling minimizes electron−hole recombination phenomena, thus resulting in a higher carrier concentration.[14] Finally, it is worth observing that the TiO_2 dopant in ZnO matrices acts itself as a catalytic promoter, favoring surface reactions between the target gases and the oxygen species adsorbed on the sensor surface.[5,13,14]

The reversibility and repeatability of these sensors were also satisfactory, as observed by repeating the tests many times without detecting any significant variation in the functional response.

To obtain a deeper insight into the system behavior, attention was focused on the analysis of the sample 3 response, which resulted in being the most efficient in gas detection. The response of this specimen toward selected analyte concentrations is reported in Figure 7. As can be observed, the obtained values increased monotonically with the operating temperature for both acetone and ethanol, in agreement with recent work by some of us,[55] due to the enhanced reactions between analytes and adsorbed oxygen species at higher temperatures. While the highest responses were registered for acetone, in the case of ethanol, the response varied from 1.3 to 5.5, which are quite good values despite the moderate working temperatures.[45] As concerns CO detection, a response decrease was observed at 400 °C, in accordance with previous reports.[44,55]

(55) Comini, E.; Faglia, G.; Ferroni, M.; Sberveglieri, G. *Appl. Phys. A: Mater. Sci. Process.* **2007**, *88*, 45.

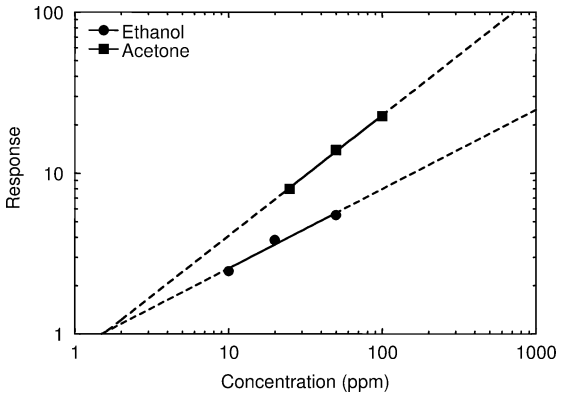

Figure 8. Response of a selected ZnO−TiO$_2$ system (sample 3, see Table 1) vs ethanol and acetone concentration at a fixed working temperature of 400 °C.

The sensor response was also investigated as a function of gas concentration, yielding a dependence obeying the typical relation for semiconductor metal oxide sensing devices:[56] response = A[gas concentration]^B, where B may have rational fraction values (usually 1 or 1/2), depending on the charge of the surface species and the stoichiometry of the involved elementary reactions. As can be observed in Figure 8, the response showed no evidence of saturation throughout the investigated concentration range. The response values can be considered good with respect to literature data, also taking into account the moderate operating temperatures with respect to those commonly adopted.[15] Remarkably, the obtained data were comparable[14,18] or even higher[18,19,57,58] than those reported in the detection of similar analytes even for pure ZnO. This feature could be traced back to the peculiar morphology and nanostructure of the obtained systems,[18,21,22] which resulted in a magnification of the measured sensitivity. On the basis of the experimental trends reported in Figure 8 and assuming the validity of the previous power law even at low gas concentrations, detection limits as low as 1.5 ppm can be expected in both cases. It is worth observing that the actual value required for a breath analyzer is 200 ppm,[16,45] underlining the impact and validity of the present results for the development of gas sensing devices with improved performances.

(56) Madou, M. J.; Morrison, S. R. *Chemical Physics of Surfaces*; Academic Press Inc.: New York, 1988.
(57) Rao, B. B. *Mater. Chem. Phys.* **2000**, *64*, 62.
(58) Anno, Y.; Maekawa, T.; Tamaki, J.; Asano, Y.; Hayashi, K.; Miura, N.; Yamazoe, N. *Sens. Actuators, B* **1995**, *24−25*, 623.

Conclusion

This work was devoted to the synthesis of ZnO−TiO$_2$ nanocomposites by a CVD route consisting of the initial deposition of ZnO NPTs (host), followed by the dispersion of TiO$_2$ (guest) in a subsequent step. The adopted procedure, which, to the best of our knowledge, has no literature precedents, is based on the synergy between the ZnO matrix porosity and the inherent infiltration power of CVD techniques, resulting in a controllable guest dispersion in the host matrix. The syntheses were performed on Si(100) and Al$_2$O$_3$ substrates under mild conditions, aimed at obtaining porous systems endowed with optimized chemico-physical properties for application in gas sensing devices.

The obtained results demonstrated that the adopted strategy is an amenable pathway to tailor the mutual ZnO/TiO$_2$ content by simple variations of titania deposition time. The use of processing temperatures lower than 500 °C enabled us to avoid undesired solid-state reactions between the two oxides, leading to Zn−Ti−O ternary phases. Furthermore, the method proved to be extremely versatile to achieve an easy control of the system morphology, structure, and chemical composition. As a matter of fact, all the obtained systems were characterized by a high purity, a significant lateral homogeneity, and a morphology/composition both dependent on the TiO$_2$ content and the ZnO matrix porosity.

Gas sensing tests pertaining to the detection of VOCs (CH_3COCH_3, CH_3CH_2OH, CO) evidenced superior functional performances with respect to the pristine ZnO NPT systems, attributable to both a sensitizing effect of TiO$_2$ particles and a higher oxygen deficiency of the composite systems. It is worth observing that, despite the moderate working temperatures, the obtained systems displayed appreciable response values. These results pave the way to the development of more efficient gas sensors working under softer conditions than the conventional ones.

Acknowledgment. This work was financially supported by Research Programs CNR-INSTM PROMO, COFIN-PRIN 2005, and FIRB-MIUR RBNE033KMA "Molecular Compounds and Hybrid Nanostructured Materials with Resonant and Nonresonant Optical Properties for Photonic Devices".

CM701990F